International Journal of Fatigue, Volume 141, December 2020, 105890
DOI:10.1016/j.ijfatigue.2020.105890

Optimised laser peening strategies for damage tolerant aircraft structures

D Busse[1,2], S Ganguly[1], D Furfari[2], P E Irving[1*]

1, School of Aerospace, Transport and Manufacturing, Cranfield University, Cranfield, MK43 0AL, UK;

2, Airbus Operations Gmbh, Kreetslag 10, Hamburg 21129, Germany

** Corresponding author; p.e.irving@cranfield.ac.uk*

Abstract

Simulation models were constructed to explore the influence of compressive residual stress on fatigue crack growth rates in aluminium sheet. Balanced residual stress fields resulting from imposition of compressive stresses in laser peen patches were calculated. Growth rates of cracks approaching, traversing and propagating away from peen patches were calculated using modified superposition models. Effects of patch dimensions and position on residual stress fields, growth rates and life were investigated. Overall life varied widely depending on the balance between retardation and acceleration; many peen arrangements had little or no life benefit. Implications of the results for damage tolerant design are discussed.

Key words

Laser peening, residual stress field, fatigue crack growth, modified superposition, damage tolerance design

1.0 Introduction & Background

Surface treatment of metallic components using laser peening has been the subject of intensive research over the past 40 years [1, 2]. The process improves fatigue life and reduces fatigue crack growth rates by inducing compressive residual stresses in the component surface and subsurface layers. Reduction

of fatigue crack growth rates is of particular importance, as the significantly increased strength of modern aluminium alloys has not been accompanied by improved resistance to fatigue crack growth.

In laser peening a series of overlapping laser pulses delivered in a raster pattern is applied to the surface of the component. The energy, size and degree of overlap of the laser pulses varies widely, depending on the peening process details. The laser pulse creates a pressure pulse of plasma at the sample surface, in turn causing local plasticity and generating an elastic residual stress field in response to the irreversible plastic mismatch strain. The benefits of laser peening over other forms of surface treatment include better surface finish and a deeper residual stress field, both of which promote longer fatigue lives [3, 4].

Previous research on fatigue crack growth in Compact Tension (CT) and Centre Crack Tension (CCT) samples of aluminium, titanium and steel positioned laser peened areas at identical positions on each sample face. Measurements of residual stresses at or near the surface of the peen patches using hole drilling, neutron diffraction and synchrotron x-rays reveal an approximately uniform compressive biaxial residual stress field across the patch, with the larger principal component in the raster direction and the smaller one perpendicular to it [5-9]. In aluminium depending on the laser conditions, subsurface compression stresses typically attain a maximum of 100-400 MPa between 0.1 and 0.2 mm depth, moving towards tension at greater depths. Often there can be tensile stresses in the interior of the sample [7, 9-11]; the extent of this interior tensile region increasing with increasing thickness. In thin samples (1.6-2.0 mm), compressive residual stresses can be maintained throughout the thickness, but are reduced in the centre [8, 11]. The peened compression region is surrounded with balancing tensile stresses both in the sample interior and at the surface [7-9] as shown in Figure 1. A fatigue crack tip approaching a peened area will first propagate in a surface tensile field (termed region 1 in Figure 2), then in a compressive field as it traverses the peened area (region 2) and finally in region 3 where the crack tip will be in tension, but with compression remaining in the peen patch behind the tip. Fatigue crack growth modifies the residual stress field from the uncracked case, but does not change the essentials of this picture e.g. [12].

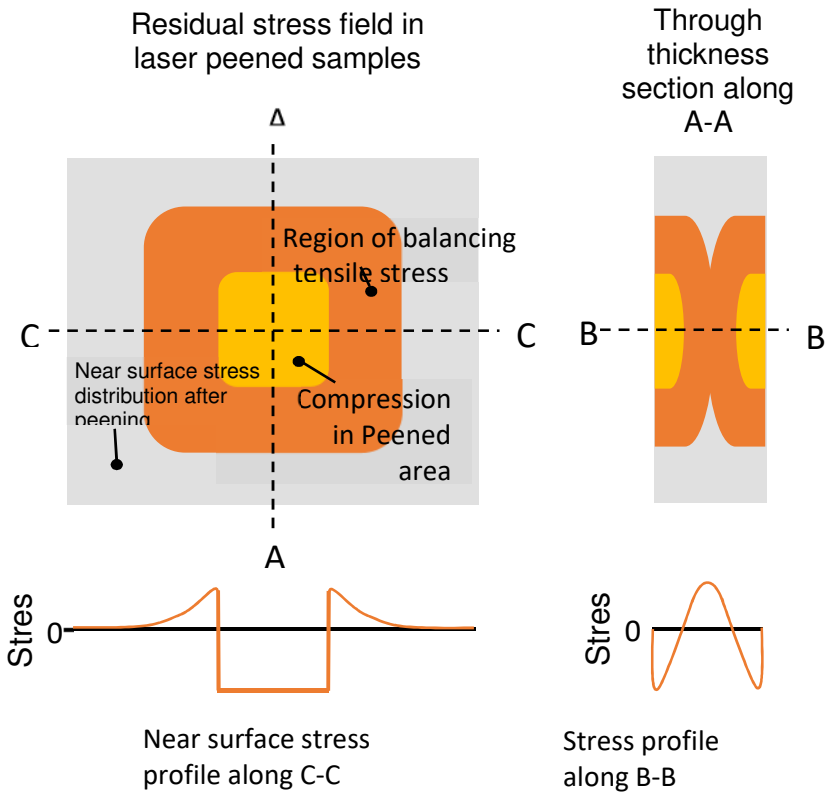

Figure 1 Schematic diagram of residual stresses after double sided peening showing distribution of compression and balancing tensile stresses; on the left near surface; on the right, through thickness; [7-9, 12 and others].

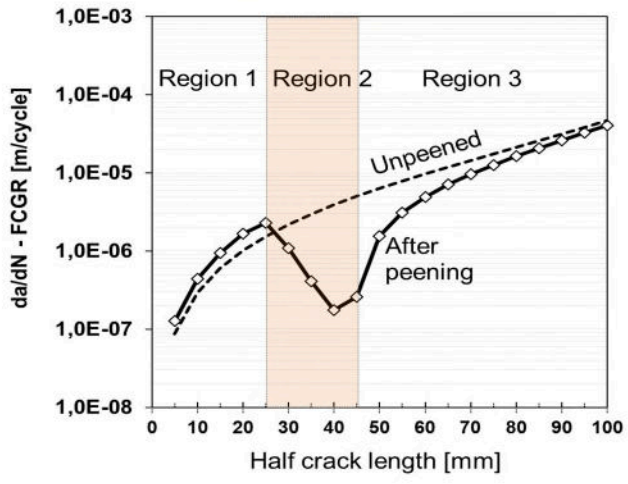

Figure 2 Schematic plot of crack growth rate vs crack length for a crack approaching a peened area (Region 1, traversing it, Region 2, and propagating beyond the patch (Region 3).

As the crack tip approaches, traverses and grows away from the peen patch fatigue crack growth rates show little or no modification in thick 10-25 mm plate [10, 13] compared with rates in unpeened material. In samples 1.6 to 6 mm thick [7-9, 14] in the tensile field of region 1 a small increase in da/dN is found, in region 2 a steady reduction in da/dN occurs with a minimum towards the peen region edge, and in region 3 a gradual increase in *da/dN* occurs eventually approaching growth rates in an unpeened sample (Figure 2).

As the crack propagates through the three regions crack closure measurements using compliance and DIC techniques [12, 14] have demonstrated that reductions in da/dN in the peened area are associated with changes in K opening (K_{op}) and enhanced crack closure in the surface regions of the sample. The lack of effect of laser peening on da/dN in thick samples can be understood as a consequence of the relatively large interior crack front length which is subject to tensile residual stress and is not subject to enhanced crack closure occurring in the surface regions. Closure behaviour dominates in relatively thin (2-6 mm) samples and crack retardation is observed e.g. [7-9, 12]. In region 3 the crack tip is once again subject to tensile stresses, but behind the tip closure of crack flanks in the peen patch occurs [8,9,12].

Simulation models- previous studies

Development of models to predict peen residual stress fields and their effect on crack growth rates has reached a high level. Four model stages are required.

(1) Calculation of local plastic strain fields developed in the peen process.

(2) Calculation of a complete residual stress field within and surrounding the peen patch.

(3) Crack introduction and calculation of ΔK_{eff} and R_{eff}.

(4) Calculation of local fatigue crack growth rates in response to the ΔK_{eff}, R_{eff} values.

In Stage (1) current techniques- for example [9, 14] for peen process simulation use first an explicit (dynamic) finite element analysis to simulate the interaction of the plasma pressure pulse produced by the laser with the material at the surface. Imposed strain rates are of the order of $\dot{\varepsilon} = 10^5$-10^6/sec with a material model to represent the material response. Once the initial pulse and elastic wave propagation

is finished, an implicit FE model is used to calculate subsequent elastic redistribution of stress. The residual stress distribution is the static elastic response of the sample to the local surface plastic misfit or eigenstrain. Experimental measurements of the residual stress field are generally used to adjust constants in the material model and pressure pulse characteristics to obtain satisfactory agreement between predicted and measured stresses.

Once these parameters are calibrated and the local plastic strain and associated stress calculated, in stage (2) the complete balanced residual stress field may be derived. Residual stress fields derived in stage (1) or from measurement are invariably incompletely known, and when introduced into an FE model will be rebalanced. This may result in local stresses significantly different from those measured. Lei et al [15] proposed the use of a proportional integral approach in which the rebalanced field is iteratively modified to create a balanced field retaining the measured or specified stresses in the peen patch. This approach has been used by Pavan and others [7, 9] to derive balanced residual stress fields consistent with incomplete measured, calculated or specified stresses. The effect on the elastic residual stress field of changes in peened area dimensions, location and component geometry may be calculated for the same eigenstrain or local peen stress input [14].

In stage (3) the crack is introduced and stress intensities calculated using a suitable technique such as Modified Virtual Crack Closure (MVCC) [23]. Simulation models using superposition of stress intensities are well established and have been shown in the modified form to give good accuracy for prediction of *da/dN* [7-9, 16-19]. The approach calculates total stress intensity values $K_{max,TOT}$ and $K_{min,TOT}$ at maximum and minimum fatigue loads resulting from the combined external and internal (residual) stresses. The external stress intensities, $K_{max,ext}$, $K_{min,ext}$ are always positive, the residual stress intensity K_{res} may be positive or negative.

$$K_{max,TOT} = K_{max,ext} + K_{res} \quad \text{E1}$$

$$K_{min,TOT} = K_{min,ext} + K_{res} \quad \text{E2}$$

The effective range of stress intensity (ΔK_{eff}) is given by

$$\Delta K_{eff} = K_{max,TOT} - K_{min,TOT} = K_{max,ext} - K_{min,ext} \quad \text{E3}$$

Similarly the effective R ratio (R_{eff}) is $R_{eff} = \frac{K_{min,TOT}}{K_{max,TOT}} = \frac{K_{min,ext}+K_{res}}{K_{max,ext}+K_{res}}$ E4

ΔK_{eff} is thus unaffected by K_{res}, whereas R_{eff} changes significantly. For situations where K_{res} is negative it is possible that $K_{min,TOT}$ as defined by E2 may be become negative. This physically unreal situation is avoided by introducing rigid crack faces into the FE model which cannot interpenetrate. Simplistically ΔK_{eff} and R_{eff} can be then calculated as follows:

$$\Delta K_{eff} = K_{max,TOT} - K_{min,TOT} \quad if\ K_{min,TOT} > 0 \quad \text{E5}$$

$$\Delta K_{eff} = K_{max,TOT} \quad \text{If}\ K_{min,TOT} \leq 0 \quad \text{E6}$$

$$R_{eff} = \frac{K_{min,TOT}}{K_{max,TOT}} \ if\ K_{min,TOT} > 0 \quad \text{E7}$$

$$R_{eff} = 0 \ if\ K_{min,TOT} \leq 0 \quad \text{E8}$$

However, when the crack is partially closed $K_{min,TOT}$ will depend on the extent of closure as well as on values of $K_{min,ext}$ and K_{res}. Equations 1 & 2 and 6-8 are only approximately correct in these circumstances. The FE model can still calculate $K_{min,TOT}$ and $K_{max,TOT}$ in the presence of partial closure and this route must be followed to obtain ΔK_{eff} and R_{eff}.

Once values of ΔK_{eff} and R_{eff} are known as a function of crack length, in stage (4) of the modelling their local values can be associated with crack growth rates (da/dN) via previously measured crack growth master curves for the material in question; the latter can be represented via the Walker [20] or similar relation between da/dN, ΔK_{eff} and R_{eff}.

Hill and Kim [19] & Pavan [7], compared experimental crack growth data from peened samples with predictions of models using simple superposition and modified superposition with crack face contact, and crack closure. Simple superposition models had worst accuracy; modified superposition gave significant improvement and good agreement with experiment. Keller [9, 12] and Hu [21] measured and modelled surface crack closure in 4.8 mm thick samples. It was demonstrated that surface residual stresses and surface crack closure were controlling crack growth behaviour, despite regions in the

sample interior being open. It was demonstrated [9, 12] that ΔK_{eff} values calculated via crack closure measurements gave equivalent accuracy of crack growth rate predictions to the modified superposition approach.

Although simulation and measurement of residual stresses and FE calculations of closure require 3D models incorporating residual stress changes with depth, simulation of fatigue crack growth in all approaches is two dimensional; the through thickness variation in residual stress being either averaged to a single equivalent value [7,8] or near surface crack face contact is calculated or measured [9,12,21]. The thinner the test sample the closer the approximation to a 2 D situation and the stronger the fatigue crack delay. Thicker samples of 10 and 25 mm thickness have little or no crack retardation reported [10, 13].

Despite the large number of published studies demonstrating the benefits of laser peen treatment on fatigue crack growth, and the availability of models which accurately predict fatigue crack growth rates in response to peen induced residual stress fields, there is no systematic study of the influence of the many parameters which an aircraft design would require for specification of a laser peen treatment to improve damage tolerance.

In this work, the roles of residual stress, peen patch location, patch geometry and externally applied cyclic stress in determining crack retardation and crack growth life on laser peened samples have been explored using a 2D FE model of a Centre Cracked Tension (CCT) panel 800 mm X 400 mm of 2524 aluminium sheet. The accuracy of the model was assessed by comparing predictions with fatigue crack growth rates measured on laser peened CCT samples of 1.6 mm 2524 T351 800 mm X 400 mm sheet for which the residual stress field had been measured using neutron diffraction.

2.0 Model description and assumptions

Simulation of laser peen processes was outside the scope of this research and was not performed. A 2D FE model of a CCT panel 800 mm X 400 mm simulated the elastic residual stress field responses to selected local compressive stresses input into peened areas within the panel. After calculation of the balanced stress field, a 6 mm half-length centre crack was introduced into the same FE mesh by

progressively relaxing nodes. The residual stress field was rebalanced and maximum and minimum external fatigue loads applied. Values of $K_{max,TOT}$ and $K_{min,TOT}$ were calculated using the MVCC technique [23]. The crack was extended a further increment, and the process repeated up to a crack length of 100 mm. Values of ΔK_{eff} and R_{eff} were calculated using equations E5 and E7. Values of *da/dN* were calculated from the ΔK_{eff} and R_{eff} values using previously determined fatigue crack growth data for a range of R ratios measured on an unpeened 800 X 400 mm 2524 1.6 mm sheet. The crack growth data were represented by the Walker equation [20].

A 2D model for residual stress field calculation was selected to avoid the complexity and large CPU calculation times of a 3D model when a large parameter space was to be explored. As noted in the introduction, published predictions of crack growth rates within laser peened samples effectively use a 2D approach and obtain accurate predictions using a single value (or an equivalent through thickness average) to represent the residual stress acting on the entire crack front.

A selected equivalent residual compression stress typical of those reported for aluminium laser peening was introduced into the area within the FE model representing the peen patch. The introduced peen stress represents the local stress associated with surface plasticity induced by laser pulse. Previous measurements and calculations suggest the stress is macroscopically uniform across the majority of the peen surface [7, 8, 14], and was assumed constant in this work for simplicity. Other stress profiles could be introduced in further work. Although the peen residual stress field is a biaxial one, only the component perpendicular to the crack plane was introduced. Following the approach of Acintha and of Lei [14, 15], once the local peen stress is defined, the remote residual stress field will be a function of the location and dimensions of the peen patch together with the sample geometry. The balancing stress field for each geometry was calculated using the iterative approach described by Lei et al [15]. Following the first calculation of the balanced stress ($\sigma_{yy,out}$), this was compared with the original input stress at the peen patch $\sigma_{yy,targ}$. If $\sigma_{yy,out} \neq \sigma_{yy,targ}$ a proportional integral (PI) controller was applied to modify initial stress values and define a new input stress ($\sigma_{yy,inp}$) according to

$$\sigma_{yy,inp}^{i+1} = \sigma_{yy,inp}^{i} + \beta(\sigma_{yy,targ} - \sigma_{yy,out}^{i}) \qquad \text{E9}$$

The iteration was repeated until $\sigma_{yy,out} = \sigma_{yy,targ}$. Full details are given in [22].

2.1 FE model details

ABAQUS 6.13-1 was used for FE analysis and the calculation of stress intensity factors. As the CCT sample is symmetric about the centreline in both X and Y directions, only one quarter was modelled (Figure 3). The centre crack introduced after stress balancing was of half - length 6 mm. Figure 3 shows sample constraints and meshing details. Elements were 2D quadrilateral S4R finite membrane strain with reduced integration. Symmetry boundary conditions were applied by rigidly fixing all nodes along

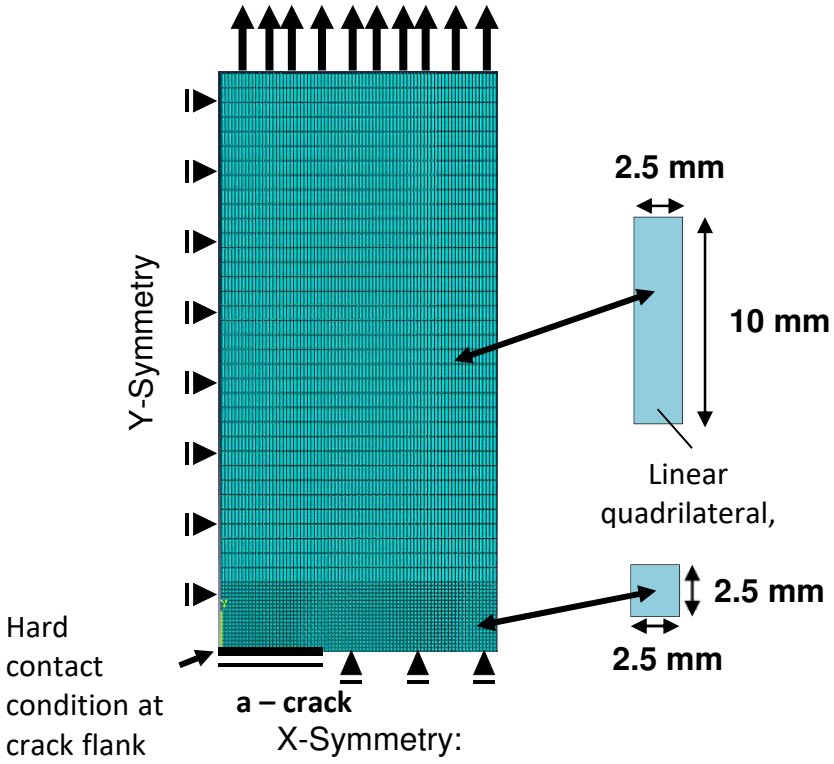

Figure 3 FE model dimensions, mesh and boundary constraints for one quarter CCT sample.

the X and Y symmetry line and allowing only movements in the direction of the symmetry line. The analysis was linear elastic in plane stress. Hard contact at the crack flanks was defined to stop interpenetration of the crack faces should displacement of nodes along the crack flanks be ≤ 0. Residual stresses were introduced into the model using the ABAQUS user subroutine SIGNI.

2.3 Calculation of crack tip stress intensities

Total stress intensities ($K_{max,TOT}$, $K_{min,TOT}$) for the crack tip under maximum and minimum external stresses σ_{max} and σ_{min} plus the residual stress field σ_{res}, were calculated using the MVCC technique [23]. Crack introduction and crack advance were simulated by releasing nodes on the X symmetry line in increments of 5 mm, up to a half crack length of 80 mm. For each crack length the nodal force (F_y) at the crack tip and the nodal displacement (u_y) at the element before the crack tip were extracted to calculate $K_{max,TOT}$ and $K_{min,TOT}$ via the MVCC procedure. Values of stress intensity $K_{max,ext}$, $K_{min,ext}$ due to external loads, and K_{res} due to residual stresses were not calculated as their values, particularly at minimum load will depend on the extent of crack contact. Values of ΔK_{eff} and R_{eff} were calculated via equations E3 & E4. After each crack increment a new calculation of the balanced residual stress field was made and was used for the new stress intensity calculation. The accuracy of the stress intensity calculation was checked against analytical results [24] and was correct to within 1%. Further modelling details are provided in [22].

2.4 Peen patch location and dimensions in the FE model

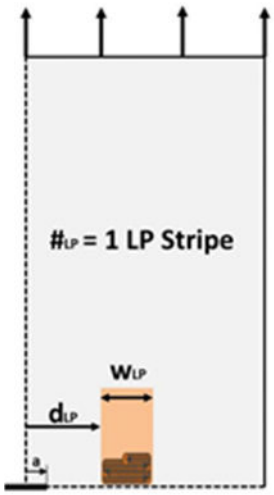

Figure 4 Diagram showing positions of peen patch in relation to the sample centre; definition of d_{lp}, w_{lp}.

Figure 4 shows schematically the peened area of width W_{lp} located at a distance of d_{lp} from the centreline. The half-length of the peen patch was 50 mm. W_{lp} and d_{lp} were systematically varied with W_{lp} values of 20, 30 and 40 mm and d_{lp} values between 25 and 65 mm.

2.4 Material properties and stress input values

Values of Young's Modulus for aluminium 2524 of 70.5 GPa and Poisson's ratio of 0.33 were used. Based on published typical data for equivalent/average laser peen residual stress values in aluminium alloys [7-9, 11], selected values for σ_{res} in the longitudinal Y direction within the peen patches were -100 MPa, -130 MPa and -150 MPa. The majority of simulations used -130 MPa. External cyclic stresses were selected to represent the Ground-Air-Ground (GAG) cycle in an aircraft fuselage, namely maximum stress σ_{max} = 90 MPa with R ratio = 0.1. For certain simulations, d_{lp} and w_{lp} were fixed and the external stress $\sigma_{max,ext}$ was changed to values of 60, 90 and 120 MPa, maintaining R ratio = 0.1,

The relation between fatigue crack growth rates da/dN and values of ΔK_{eff} and R_{eff} for the aluminium alloy 2524 in 1.6 mm sheet was represented using the Walker equation [20].

$$\frac{da}{dN} = \frac{C_0(\Delta K_{eff})^m}{(1-R_{eff})^{m(1-n)}} \qquad \text{E10}$$

Where C_0, m and n are constants determined by curve fitting from constant amplitude fatigue crack growth tests on unpeened material over a range of R ratio values. To determine values of C_0 m and n, constant amplitude fatigue crack growth tests were conducted on CCT samples of 2524 aluminium 800 mm X 400 mm, 1.6 mm thick, in accordance with ASTM E647 recommended procedures. The rolling direction was perpendicular to the loading axis (T-L direction) [22] and the UTS and proof strength were measured as UTS= 413 MPa, 0.2% proof = 290 MPa and elongation was 7%. Two identical samples were tested at each R value of 0.1, 0.3 and 0.5; crack growth was monitored using a travelling microscope and values of crack length and cycles were recorded at regular intervals. Fatigue crack growth rates were calculated using finite difference following ASTM E647 procedures. Values of C_0 m and n for the Walker equation, obtained from curve fitting crack growth rate and stress intensity data, were $C_0 = 1 \times 10^{-7}$ m/cycle, m= 2.86 and n = 0.59. Complete test and sample details can be found in [22].

3.0 Simulation results

3.1 Balanced stress distribution around peen patches before crack introduction

An example of an initial unbalanced and a final balanced stress field for the σ_{yy} component after iteration is shown in Figure 5. The compression stress field is maintained within the peen patch but is no longer completely uniform. The balancing tension field surrounds the peen patch, with largest values adjacent to it, diminishing to zero as the sample edge is approached. Large stress gradients are predicted at the peen patch boundaries. The field is L-R asymmetric as only one half of the sample is modelled.

Figure 6 shows calculated residual stress profile on the sample transverse centreline (crack line) for two positions of the peen patch. Within the peen patch there is almost uniform -130 MPa. Outside is the balancing tensile field which changes with patch position, having a maximum of 40 MPa for d_{lp} = 25 mm. For d_{lp} = 65 mm, the maximum is reduced to 25 MPa. The tensile field is again asymmetric, with greater stresses on the centreline side.

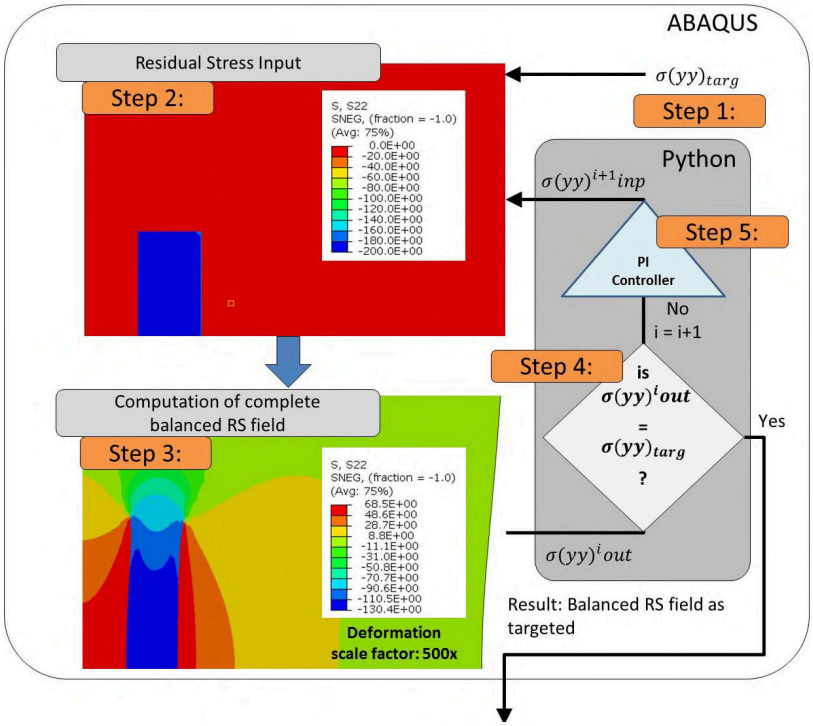

Figure 5 2D FE simulation of quarter CCT sample, before and after stress balancing. peen patch (blue) has uniform residual stress of 130 MPa compression, surrounded by zero stress field red; (b) Balanced residual stress field after iterations with balancing tensile stress in red with compression stress 130 MPa.

Effect of peen patch position on stress distribution

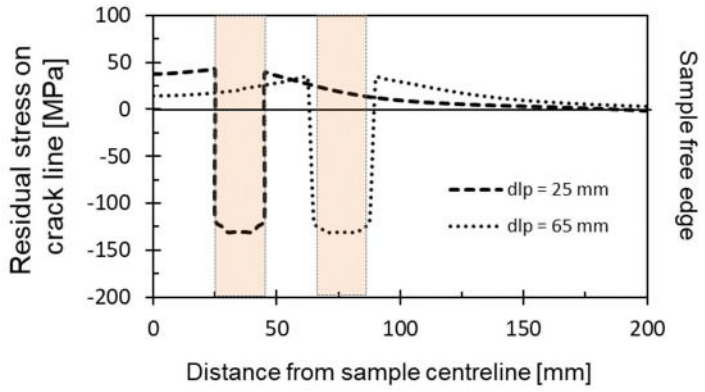

Figure 6 Profile of longitudinal residual stress on the crack line showing compressive residual stresses of 130 MPa within peen patch with balancing tensile stresses on either side. W_{lp} = 20 mm. Comparing tensile response with d_{lp} values of 25 and 65 mm.

Effect of peen patch compressive stress

Increasing the compressive stress within the peen patch from -100 MPa to -150 MPa increases slightly the maximum tensile stress (Figure 7). However the increase is roughly a quarter of the increase in compressive stress as the tensile balancing forces are spread over a larger area.

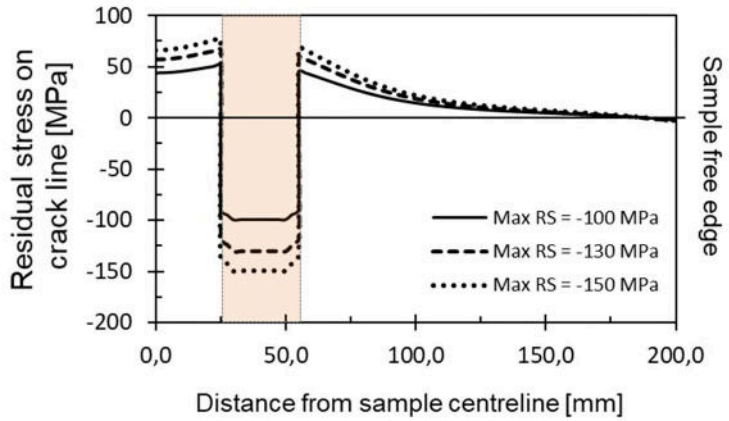

Figure 7 Influence of compression stress of 100, 130 and 150 MPa. Residual stress profile on crack line, w_{lp} = 30 mm, d_{lp} = 25 mm.

Effect of peen patch width

Increasing the peen patch width from 20 to 40 mm maintaining the same compression stress has a powerful effect on the balancing tensile field. Figure 8 shows the maximum tensile stress increases from 40 to over 90 MPa as the peen width is doubled. This large effect, even though the compression stress is unchanged, is a consequence of the requirement to balance the larger area of compression stress as w_{lp} increases with a reduced unpeened area.

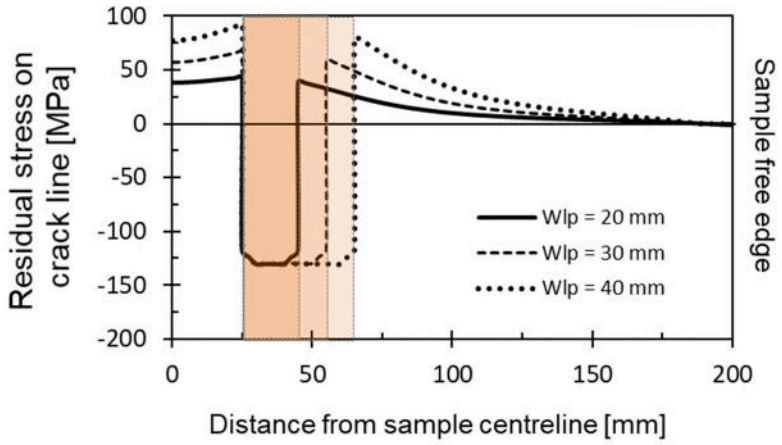

Figure 8 Residual stress profile on crack line d_{lp}= 25 mm, w_{lp} values of 20, 30 and 40 mm; residual stress value 130 MPa compression.

3.2 Residual stress field changes with crack growth

Calculated values of σ_{res} on the crack line at half crack lengths of 0, 20, 40, and 70 mm are shown in Figure 9 under an external minimum stress of 9 MPa. The 3 crack tip positions are located before, within and beyond the peen patch.

Crack growth to 20 mm (Figure 9b) removes the tensile stresses before 20 mm and reduces the compression stress in the peened area, while increasing tensile stresses in region 3, as balancing tensile stresses can be located only in this uncracked region. The tip of the 40 mm crack (Figure 9c) is in the peen patch compression field. Compressive stresses can act across the crack faces. Residual stresses

between a = 25 mm and 40 mm are reduced. Tensile stresses in region 3 are reduced but still greater than in the uncracked situation. The 70 mm crack has the tip in tensile stresses in region 3 and. Although the tip region is in tension, crack faces within the peen patch behind the tip still bear compression stresses, and will maintain R_{eff} =0 and reduce ΔK_{eff} despite the tension field surrounding the tip.

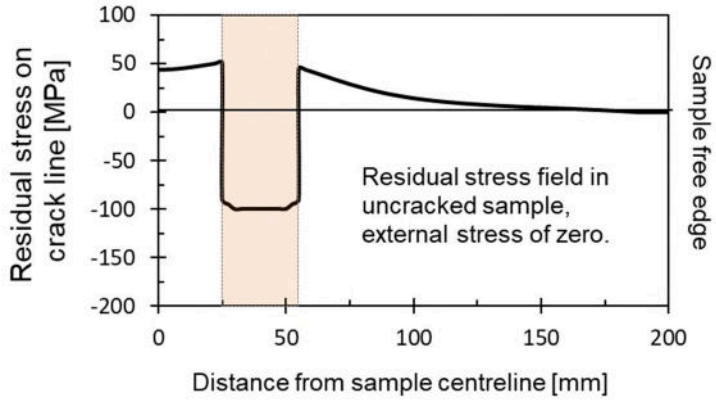

Figure 9(a) Uncracked residual stress field; external stress of zero.

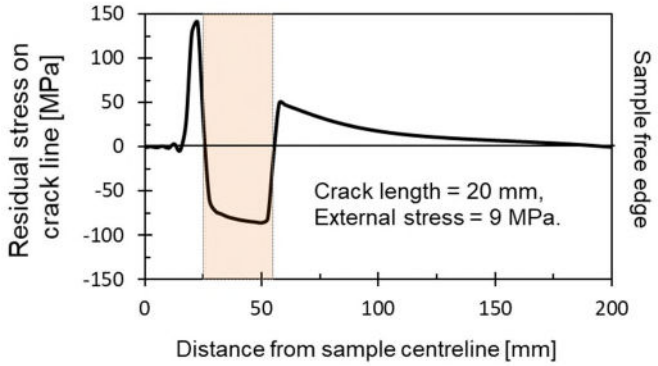

Figure 9(b) Half crack length = 20 mm, external stress 9 MPa.

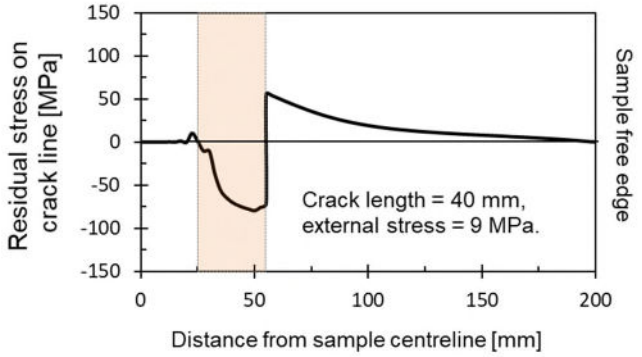

Figure 9(c) Crack length =40 mm, external stress 9 MPa.

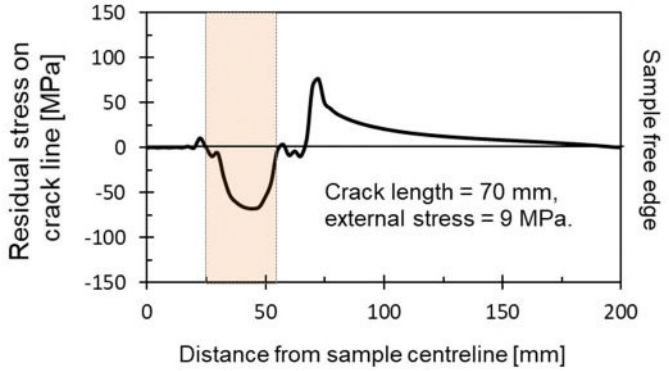

Figure 9(d) Crack length =70 mm, external stress 9 MPa

Figure 9 Effect of crack growth on introduced residual stress; stress profiles on crack line (a) original uncracked; (b), (c), (d) half crack length of 20 mm; 40 mm; 70 mm respectively; σ_{res} = 100 MPa compression, w_{lp} = 30 mm, d_{lp} = 25 mm; peened region shaded.

3.3 Effect of residual stress field on ΔK_{eff}, R_{eff}, and crack growth rates da/dN

Figures 10 a, b and c shows the predictions of ΔK_{eff}, R_{eff} and growth rate *da/dN* for a single peen patch, d_{lp} = 25 mm and w_{lp} = 30 mm. External cyclic stresses were σ_{max} = 90 MPa and R=0.1. σ_{res} in the peen patch was set at 100, 130 and 150 MPa compression. Baseline values without a peen patch for ΔK and *da/dN* are also shown in figures 10a and 10c.

Figure 10a shows increases in ΔK_{eff} with increasing crack length up to a half crack length of 30 mm, about 5 mm inside the peen patch boundary. Up to this point the baseline and peened sample ΔK_{eff}

values are identical. ΔK_{eff} reduces after this point reaching a minimum about 5 mm prior to the crack tip emerging from the peen patch. The reduction in ΔK_{eff} is greatest for the largest compressive residual stress, and least for the smallest. After this point ΔK_{eff} increases, approaching but not achieving the baseline value.

In the region before the peen patch, there are tensile residual stresses and R_{eff} (Figure 10b) is increased from the nominal 0.1 to between 0.4-0.5. Within the peen patch R_{eff} reduces rapidly to zero for the entire width of the patch, prior to increasing to R_{eff} of 0.2-0.3 when the crack tip emerges. *da/dN* values in da/dN values in Figure 10c closely follow changes of ΔK_{eff} in Figure 10a. Figure 10c shows a small increase in crack growth rate in the high R_{eff} region before the patch, followed by a decrease of up to a factor of 50 within the patch. Beyond the patch growth rates rapidly increase, approaching but not achieving baseline values. The simulations with larger compressive residual stresses cause increased balancing tensile stresses and larger values of R_{eff} in the region before the patch. There is no change in ΔK_{eff} (see equation 3) but there will be increased *da/dN* due to the larger R_{eff}.

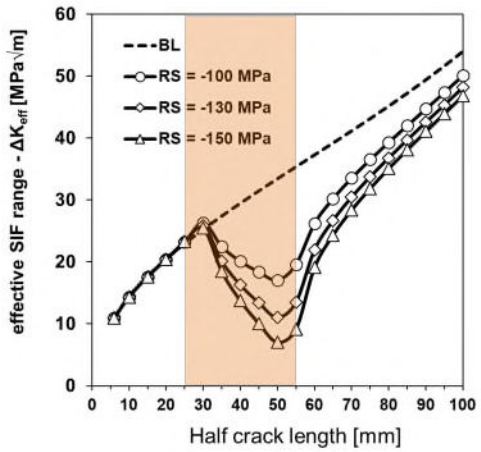

Figure 10a

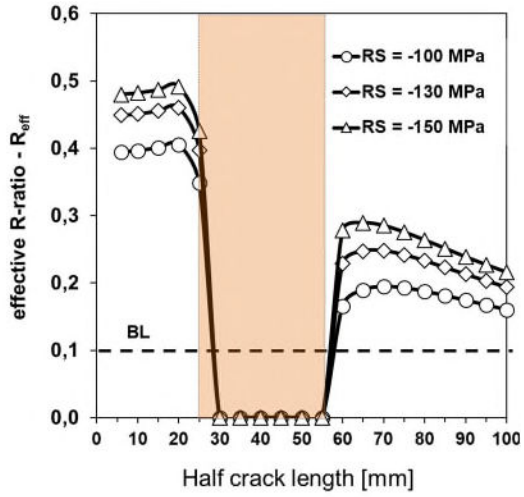

Figure 10b

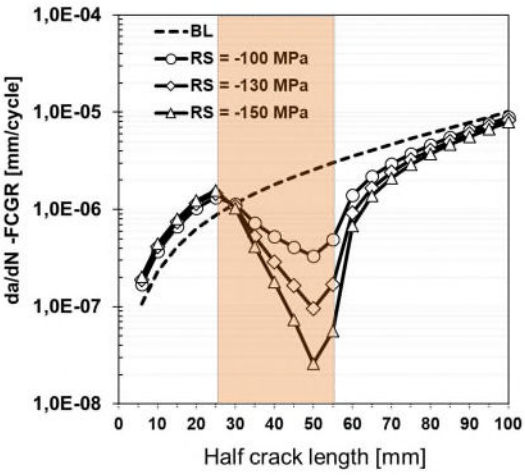

Figure 10c

Figure 10 Predicted Changes with crack length of (a) ΔK_{eff}; (b) R_{eff}; (c) da/dN; d_{lp} = 25 mm, W_{lp} = 20 mm, comparison of σ_{res} = 100, 130 and 150 MPa compression.

Effect of changes in w_{lp} and d_{lp} on predicted fatigue crack growth rates

da/dN values vs. half crack length are shown in Figure 11(a) for d_{lp} held constant = 25 mm while w_{LP} values were 20, 30 and 40 mm, and 11(b) for w_{LP} = 20 mm, and d_{lp} values increased from 25 mm to 65 mm. Increasing w_{lp} increases the distance over which compressive residual stress operates and further reduces values of *da/dN*. Greatest peen patch width gives slowest minimum growth rates and the largest

section of retarded growth. At the same time there are increased tensile stresses in regions 1 and 3 (see Figure 8) with consequential da/dN increases.

Increasing the distance of the peen patch d_{lp} from the centreline increases *da/dN* values overall. For d_{lp} = 25 mm, the *da/dN* minimum is a factor of 10 smaller than the baseline; for d_{lp} = 65 mm it is only a factor of 3 smaller. Increasing d_{lp} increases the distance through which the crack propagates in a tensile stress field.

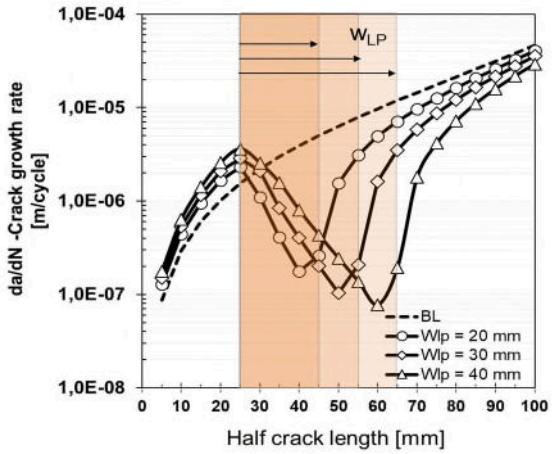

Figure 11(a)

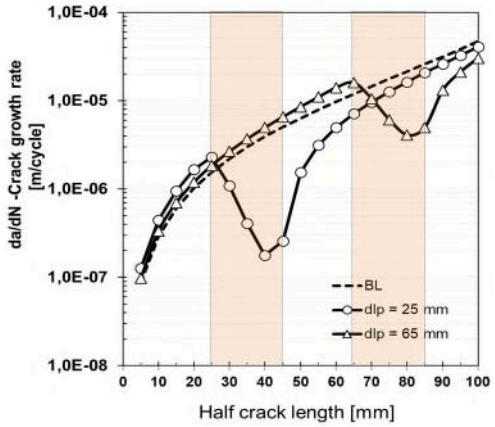

Figure 11b

Figure 11 Changes of da/dN with crack length; comparing effects of changes in w_{lp}; (a) 20, 30, 40 mm, and (b) d_{lp} (25 and 65 mm); σ_{res} = 130 MPa compression.

Effects of external loading on crack growth rates

The stress range Δσ and R ratio applied externally to the sample will influence ΔK_{eff} and R_{eff} at the crack tip and hence change *da/dN* values. The senstivity of growth rate to external loading was investigated using a peen patch with d_{lp} = 25 mm, w_{lp}=30 mm and σ_{rs} = -130 MPa. The effects on da/dN of maximum external stress values of 120 MPa, 90 MPa and 60 MPa at an R ratio of 0.1 are shown in Figure 12 in comparison with relevant base line curves.

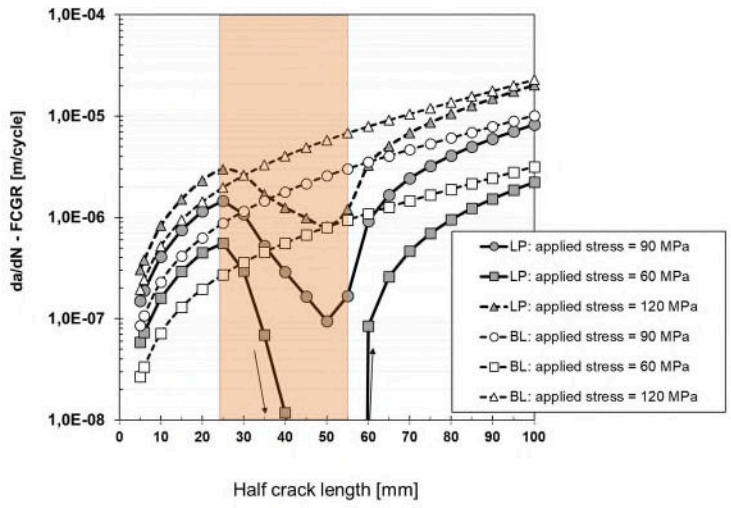

Figure 12 Effects of external cyclic stress on da/dN; Comparison of da/dN changes for σ_{max} = 60, 90 and 120 MPa; σ_{res} = -130 MPa, d_{lp} = 25 mm, w_{lp} = 30 mm.

It can be seen that decreasing the maximum cyclic stress σ_{max} of course decreases da/dN values in all three regions of crack growth; however greatest reductions are within the peen patch. Here minimum da/dN is reduced by a factor of 10 by reducing σ_{max} from 120 MPa to 90 MPa. Further reductions of σ_{max} to 60 MPa reduces minimum da/dN by several orders of magnitude, effectively producing crack arrest. Relative to the baseline, the minimum da/dN at 120 MPa is reduced by a factor of 7, at 90 MPa it is reduced by a factor of 25 and at 60 MPa the crack is arrested within the peen patch.

3.4 Effects of *da/dN* changes on sample lives

Effect of changes in d_{lp} and w_{lp} on life

The *da/dN* data shown in figures 10-12 were integrated to create crack length vs cycles data to assess the effect of changes in peening on sample lives. Because in experiments sample failure was observed at half crack lengths of approximately 80 mm, the data in 13,14 and 17 are terminated at this value. Figure 13a shows the effect of peen patch width w_{lp} and Figure 14b distance d_{lp} on life. While generally there is a significant beneficial effect of increasing peen patch width on life to achieve an 80 mm crack length, cycles to achieve smaller crack lengths of 35-40 mm are reduced compared with the baseline. This is a consequence of the increasing growth rates in region 1. Greatest final lives are produced by

the widest peen patch, but improvements in life are not achieved until a minimum crack length of 50 mm is attained. Prior to this lives are reduced, not increased.

The effects on life of increasing d_{lp} for constant w_{lp} = 20 mm are shown in figure 13b. While there are improvements in total life for the smallest d_{lp} values of 25 and 35 mm, d_{lp} values greater than this give reductions in life over the baseline unpeened data. Even for d_{lp} values of 25 and 35 mm, life improvements are found only after crack lengths have grown beyond 40-50 mm. Prior to this there are life reductions.

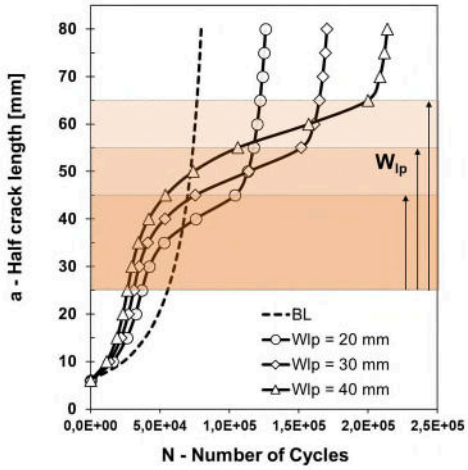

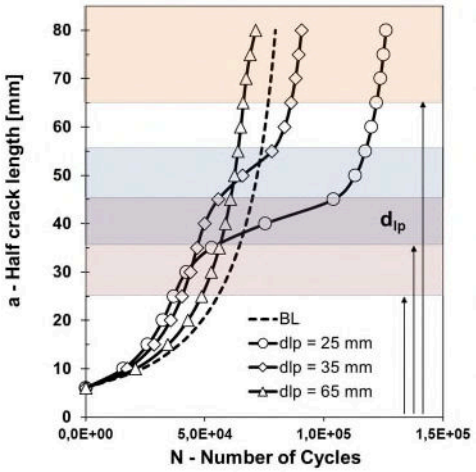

Figure 13a **Figure 13b**

Figure 13 (a) Comparison of crack length- cycles curves for w_{lp} = 20, 30, 40 mm; σ_{res} = 130 MPa, d_{lp} = 25 mm. (b) Comparison of crack length – cycles curves for d_{lp} = 25, 35 and 65 mm, w_{lp} = 20 mm, σ_{res} = 130 MPa compression.

Effects of peen compression stress; constant dlp and wlp

The effect on life of increasing the peen compression stress from 100 MPa to 150 MPa is shown in figure 14. An increase to 150 MPa compression more than triples the baseline life; there is little improvement at -100 MPa. Lives to achieve crack lengths less than 40 mm, are all reduced irrespective of the compression stress value.

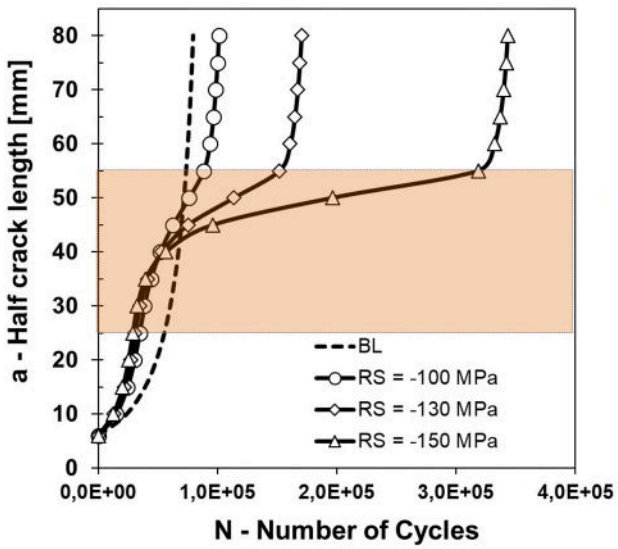

Figure 14 Crack length – cycles data for 3 different values of σ_{res} = -100, -130, and -150 MPa; d_{lp} = 20 mm, w_{lp}= 30 mm.

Effects of external stress values on cycles to achieve 80 mm length

All external stress values had reduced life up to 35-45 mm half length followed by retardation and increased life afterwards. Samples subjected to 120 MPa had a doubling of overall life compared with baseline; For σ_{max} = 90 MPa life of peened samples increased by a factor of 20 relative to the baseline. If σ_{max} was increased to 120 MPa, this was reduced to a factor of 2. For the smallest σ_{max} of 60 MPa accelerated growth up to crack lengths of 35 mm was found. After this length da/dN values were reduced to the extent that the crack was arrested and life was infinite.

4.0 Comparison of 2 D simulations with measurements of fatigue crack growth in peened samples

Sample preparation

Two identical CCT samples of clad 2524 aluminium 800 mm X 400 mm X 1.6 mm were laser peened on each surface to produce 50 mm long peen patches on each side of a central notch of 2a=12 mm (see Figure 4). For the experiments w_{lp} =30 mm, and d_{lp} = 25 mm. A Nd:YAG laser with a pulse rate of 20 Hz, a spot size of 1.5 mm, a power density of 2.5 GW/cm^2 and a pulse density of 750/cm^2 was used. Full experimental details are provided in [22]. Residual stress fields within and around the peen patches were measured using neutron diffraction at the SALSA instrument at ILL Grenoble [22]. The nominal

gauge volume of the incoming beam was set to 0.6 X 0.6 mm. Six locations in the X-Y plane were selected for stress measurement along the sample transverse centreline, 3 inside the peen patch and 3 outside (Figure 15). At each point the centre of the gauge volume was positioned to take measurements at depths in the Z direction of 0.6 mm, 0.8 mm, and 1.0 mm from the sheet surface. 300 neutron counts were taken for each measurement. All three components of stress were measured.

After measurement of residual stresses both samples were fatigue tested at 6 Hz at R = 0.1 and a maximum stress of 90 MPa using procedures consistent with ASTM E647 standard. The growth of cracks across the sample was monitored using a travelling microscope. Values of crack length and cycles were recorded at regular intervals. Full experimental details of measurement and testing are provided in [22]. After testing data was processed following ASTM E647 recommendations for finite difference.

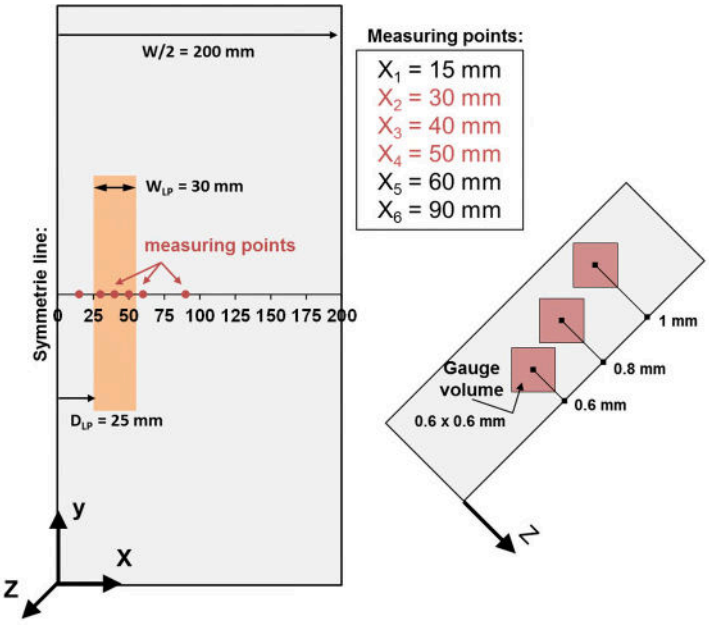

Figure 15 Schematic diagram of half of the CCT sample showing location of measurement points to define the residual stress field [22].

4.1 Experimental residual stress field measurements

Figure 16 shows measured local residual stress values perpendicular to the crack plane plotted against distance from the sample centreline. Stresses measured at 0.6, 0.8 and 1 mm depth, and their arithmetic

mean are shown at each location. Within the peen patch mean compressive stresses are greatest (70-90 MPa) near the edges of the patch; in the centre 50 MPa was found. Outside the peen patch, averaged values are tensile at 50-100 MPa close to the peen edge, declining to near zero 90 mm away frm the edge.

To explore how well the 2D iterative stress balancing procedure could calculate stress fields measured on a 3D sample, values of -130 MPa and -100 MPa were input into the model used earlier and the balanced field derived. The resultant stress profiles are also shown in Figure 16. The measured values of stress are consistent with the general shape of the theoretical curves in figure 6-9, particularly Figure 9a, as it has the correct values of w_{lp} and d_{lp} , with mean stresses at two of the 3 points outside the peened area accurately predicted. Compressive stresses in the centre could be approximated by a uniform stress of 70 MPa compression. As Figures 16 and 7 show, changes in peen patch stress alone have a relatively small influence on the balancing tension stress field. The size of the gauge volume in the z direction of 0.6 mm means that through thickness variations in residual stress will be smoothed and local stress maxima in the surface regions will not be represented.

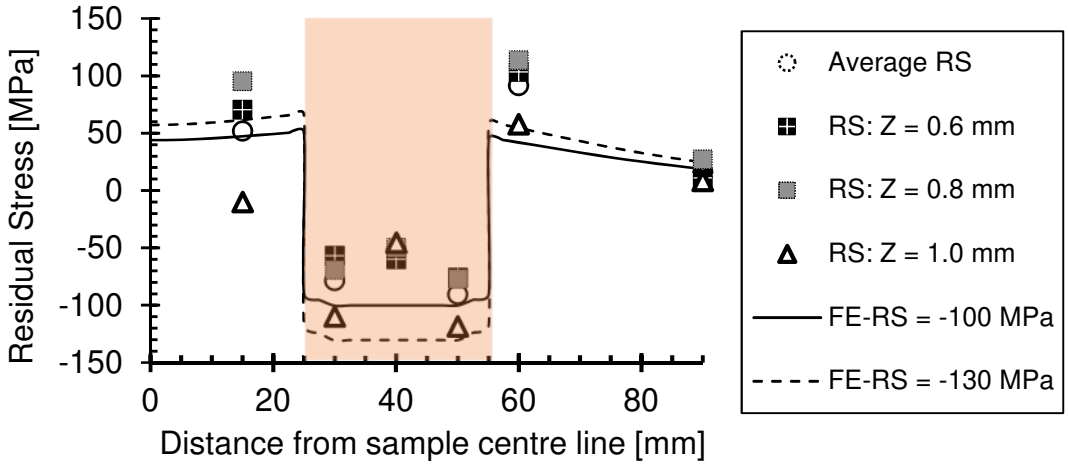

Figure 16 Comparison of measured and calculated residual stresses in peened sample of 1.6 mm 2524 aluminium; d_{lp} = 25 mm, w_{lp} = 30 mm.

4.2 Measured and predicted fatigue crack growth rates

Experimental da/dN and a vs N data from peened samples tested as described earlier are shown in Figures 17 a & b. Also shown in the figure are growth rates for the baseline material at R = 0.1 and

predicted growth rates for peen patch residual stresses of -100 and -130 MPa, taken from Figure 16. In the region before the peen patch, the experimental points closely follow the predicted increase in da/dN. Within the peen patch da/dN values reduce, reaching a minimum about 5 mm before the far edge of the peen patch, in agreement with predictions of the models . After the peen patch, da/dN increases, initially in agreement with predicted trends. Experimental data points fall within the two predicted trendlines corresponding to σ_{res} of between 100 and 130 MPa compression.

Both models and experiments show a reduction of about 50% in the number of cycles required to achieve crack length of 30 mm with models over predicting the cycles number. After 45 mm, experiments and models show an increase in overall life of 20-25% at test end. Experimental data most closely matches the predictions for σ_{res} of 100 MPa compression. A residual compressive stress of 70-80 MPa would better fit to measured peen stresses but would have worse agreement with predicted da/dN values.

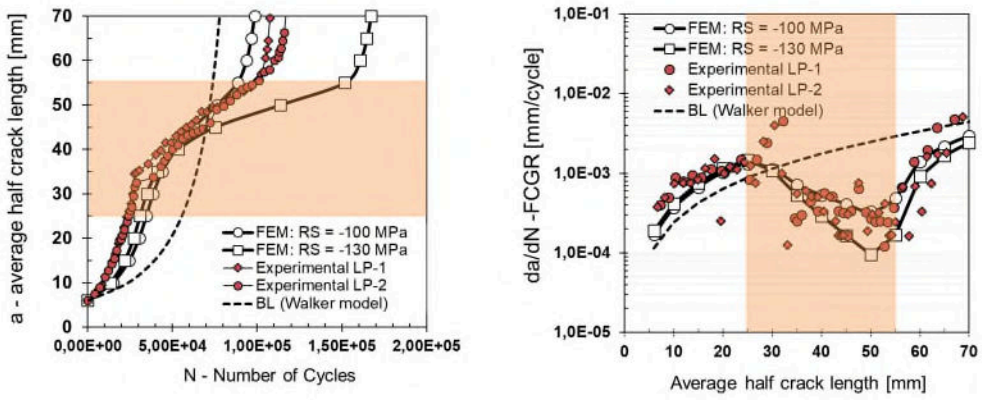

17a **17b**

Figure 17 (a) Comparison of measured and simulated crack length – cycles data; simulations assuming σ_{res} values of -100 and -130 MPa; measured residual stresses as shown in Figure 16. d_{lp} =25 mm, w_{lp} = 30 mm. (b) Comparison of measured and simulated crack growth rates from the data shown in (a)

5.0 Discussion

Comparison of experimental measurements with predicted trends using the 2D crack growth model has demonstrated that the model accurately reproduces the major features of crack growth through a

peened arrea, provided that a suitable equivalent stress value is selected to represent the 3D through thickness variation and crack face contact taking place in the surface regions. In this case the mean residual stresses measured in the peen patch -70 MPa, are smaller that the values required to give accurate predictions of growth rates. (between -100 and -130 MPa). The neutron diffraction gauge volume dimension of 0.6 mm will average the true residual stress through the thickness and it may be that smaller stresses in the interior regions are over represented. The 2D model accurately reproduces the major features of crack growth through the 3 regions peen patch reported by others [e.g. 7-9], and has allowed systematic investigation of the separate roles of residual stress value, peen width peen location and the role of external loading.

Damage tolerant design requires selection of stress levels, material crack growth characteristics and Non Destructive Test (NDT) capabilities so that propagating fatigue cracks have high probability of detection on inspection before catastophic failure.

Application of laser peen patches to slow down propagating fatigue cracks could reduce costs of maintaining damage tolerant aircraft by increasing inspection intervals or permitting use of increased design stresses for the same inspection intervals.

The important attributes of crack growth through laser peen areas relevant to damage tolerance design are:

- The length and number of cycles occupied in the initial region 1 of reduced life.
- The number of cycles of delay after this point in regions 2 and 3.

As region 3 occurs at longer crack lengths and faster growth rates, its contribution to total life is less than region 2 but still significant. In Figure 14 region 3 contributes about 30% of the total life, region 2 over 50% for the -150 MPa case, and region 1 12%. For the smallest residual sress of -100 MPa, the region 2 contribution is reduced to 30%.

Crack acceleration in region 1 is minimised by decreasing the R ratio by keeping balancing tensile stresses small; This is achieved in finite width samples by minimising peen patch width (Figures 7 &

8). Decreasing the distance from the crack tip to the peen patch minimises the cycles necessary to traverse region 1 (Figure 13b).

Crack retardation and lives in region 2 are enhanced by minimising the width of region 1. This results from a combination of the smaller period in region 1 combined with enhanced retardation in region 2. The converse is true; large values of dlp prolong region 1, increase ΔK_{ext} relative to ΔK_{res}, and therefore increase ΔK_{eff}. Figure 13b shows lives of peened samples are doubled compared with baseline for d_{lp} = 25 mm , only 25% increase for d_{lp} = 35 mm and a reduced life for d_{lp}= 65 mm as region 1 acceleration outweighs reduced retardation in region 2.

Compressive residual stress has a powerful effect on retardation and should be as large as possible (Figure 10c). Provided w_{lp} remains small, balancing tensile stresses are not significantly changed and there is only small increase in the da/dN in region 1. Overall lives are consequently significantly increased (Figure 17 showing a factor of more than 4 increase on life compared with baseline for the largest residual stress of -150 MPa). In the 3D situation, there may be adverse effects of large peening stresses on retardation if they promote increased tensile stress in the centre regions.

A further complication in exploitation of peening retardation is the sensitivity of retardation to external stress shown in this work, and to R ratio demonstrated in e.g.[9]. This behaviour implies that quantitative knowledge of the stresses in service is essential so that σ_{res} and K_{res} can be matched to the values of ΔK_{ext} so that the combined $K_{min,TOT}$ values are reduced sufficiently to cause substantial crack face contact and retardation. The retardation response to variable amplitude loading will be determined by the amplitude and R ratio content of the loading spectrum. Separate from reversed plasticity issues which may complicate thngs further, spectra consisting of low R ratio cycles such as fuselage GAG ((Ground- Air- Ground) spectra will have mores substantial retardation than wing spectra which containa both GAG and high R ratio gust loads. It may be possible to use laser peening to eliminate the contribution to crack growth of a high proportion of smaller amplitude cycles which have increased retardation, with suitable design of the peening patch.

6.0 Conclusions

(1) Systematic exploration using an FE model of the effects of peen patch location, width, residual stress field and external applied stress on crack growth rate has shown a wide range of resulting fatigue lives. A significant number of scenarios are detrimental to fatigue life.

(2) The position and extent of the peened region within the test sample influences the size and extent of the balancing tension field, even though the compression stress may be constant.

(3) Balancing tensile residual stresses in the region between the crack tip and the peen patch promote crack acceleration, and reduced life up to the point where the crack tip enters the peened area and is subsequently retarded. Whether the overall life is greater or less than that of the unpeened baseline will depend on the relative numbers of the cycles occupied in traversing the regions of tensile and compressive stresses.

(4) The region of crack growth after the peen patch, has compression stresses behind the tip. Crack retardation is maintained in this region despite the tip being in tension, although the contribution of this region to total life is .

(5) The life extension produced by single peen patches is strongly dependent on the external loading and declines in effectivness as the ΔK value increases. It will hence depend on the service loading spectrum.

Acknowledgements

Thanks are due to Yigeng Xu for assistance with interpretation of FE analysis data.

The authors would like to thank Airbus Operations for financial support and supply of material.

References

[1] Fairand BP, Williams DN, Wilcox BA, Gallagher WJ; (1972) "Laser shock-induced microstructural and mechanical property changes in 7075 aluminium" J. App. Phys. 43, p 3893.

[2] Fairand BP, Clauer AH, Jung RG, Wilcox BA; (1974) App. Phys. Lett. 25(8) p 431.

[3] Montross C, Wei T, Ye L, Clark G, Mai Y; (2006) "Laser shock processing and its effects on microstructure and properties of metal alloys: a review" Int. J. Fatigue; 24; pp 1021-1036.

[4] Gujba AK, Medraj M; (2014); "Laser peening process and its impact on materials properties in comparison with shot peening and ultrasonic impact peening" Materials; pp 7925-7974.

[5] Dorman M, Toparli MB, Smyth N, Cini A, Fitzpatrick ME, Irving PE, (2012) "Effect of laser shock peening on residual stress and fatigue life of clad 2024 aluminium sheet containing scribe defects" Mat. Sci. Eng. A548 pp 142-151.

[6] Kallien Z, Keller, S, Ventzke V, Kashaev N, Klusemann B, (2019) "Effect of laser peening process parameters and sequences on residual stress profiles" Metals 9, 655.

[7] Pavan M, Furfari D, Ahmad B, Gharghouri MA, Fitzpatrick ME (2019) "Fatigue crack growth in a laser peened residual stress field," Int. J. Fatigue 123 pp 157-167.

[8] Kashaev N, Ventzke V, Horstmann M, Chupakhin S, Riekehr S, Falkck R, Maawad E, Staron P, Schell N, Huber N (2017) "Effects of laser shock peening on the microstructure and fatigue crack propagation behaviour of thin AA2024 specimens" Int. J. Fatigue 98 pp 223-233.

[9] Keller S, Horstmann M, Kashaev N, Klusemann B, (2019),"Experimentally validated multistep simulation strategy to predict the fatigue crack propagation rate in residual stress fields after laser shock peening" Int. J. Fatigue, 124, pp 265-276.

[10] Chahardehi A, Brennan, F, Steuer A (2010); "The effect of residual stresses arising from laser shock peening on fatigue crack growth" Engng. Frac. Mech; 77; pp 2033-2039.

[11] van Staden SN, Polese C, Glaser D, Nobre J-P, Venter AM, Marais D, Okasinski J, Park J-S; (2018); Materials Research Proceedings 4 pp 117-122.

[12] Keller S, Horstmann M, Kashaev N, Klusemann B; (2019) "Crack closure mechanisms in residual stress fields generated by laser shock peening" Eng. Frac. Mech. 221, UNSP 106630.

[13] Bergant Z, Trdan U, Grum J, (2016) "Effects of laser processing on high cycle fatigue crack growth rate and fracture toughness of aluminium alloy 6082 T651", Int. J. Fatigue 87 pp 444-455.

[14] Achintha M, Nowell D, (2011) "Eigenstrain modelling of residual stresses generated by laser shock peening" J. Mat. Process Technology" 211 pp 1091-1101.

[15] Lei Y, O'Dowd NP, Webster GA, (2000) "Fracture mechanics analysis of a crack in a residual stress field" Int. J. Fract, 106, pp 195-216.

[16] LaRue JE, Daniewicz SR; (2007); "Predicting the effect of residual stress on fatigue crack growth" Int. J. Fat. 29 pp 508-515.

[17] Ma Y-e, Staron P, Fischer T, Irving PE; (2011) "Size effects on residual stress and fatigue crack growth in friction stir weld 2195 –T8 aluminium; Part II Modelling" Int. J. Fat. 33; pp 1426-1434.

[18] Garcia C, Lotz T, Martinez M, Artemev A, Alderliesten R, Benedictus R; (2016) "Fatigue crack growth in residual stress fields"; Int. J. Fat. 87; pp 326-338.

[19] Hill MR, Kim J; (2012) "Fatigue crack closure in residual stress bearing materials" J. ASTM International; 9(1) 104071.

[20] Walker EK, (1970) "The effect of stress ratio during crack propagation and fatigue for 2024 –T3 and 7075 T6 aluminium" in ASTM STP 462 Am. Soc. Test Mater. pp 1-14. ASTM.

[21] Hu Y, Cheng H, Yu J, Yao Z, (2020), "An experimental study on crack closure induced by laser peening in pre-cracked aluminium alloy 2024 T351 and fatigue life extension" Int. J. Fatigue 130 105232.

[22] Busse O, (2017) "Extending fatigue life of aircraft fuselage structures using laser peening" Cranfield University Ph D Thesis 2018.

[23] Krueger R; (2002) "The virtual approach crack closure technique: History, and applications" ICASE report. Hampton VA.

[24] Feddersen C E; (1966), Discussion in ASTM STP 410 pp 77-79; ASTM 1966.

Optimised laser peening strategies for damage tolerant aircraft structures

Busse, David Osman

2020-08-14

Busse D, Ganguly S, Furfari D, Irving PE. (2020) Optimised laser peening strategies for damage tolerant aircraft structures. International Journal of Fatigue, Volume 141, December 2020, Article number 105890

https://doi.org/10.1016/j.ijfatigue.2020.105890